

# Quantum Chemical Study of Arsenic (III, V) Adsorption on Mn-Oxides: Implications for Arsenic(III) Oxidation

MENGQIANG ZHU,<sup>\*,†</sup>  
KRISTIAN W. PAUL,<sup>‡</sup> JAMES D. KUBICKI,<sup>§</sup>  
AND DONALD L. SPARKS<sup>†</sup>

Department of Plant and Soil Sciences, Center for Critical Zone Research, University of Delaware, 152 Townsend Hall, Newark, Delaware 19716, DuPont Crop Protection, Stine-Haskell Research Center, Newark, Delaware 19714, and Department of Geosciences and the Earth and Environmental Systems Institute, The Pennsylvania State University, University Park, Pennsylvania 16802

Received February 19, 2009. Revised manuscript received June 17, 2009. Accepted July 6, 2009.

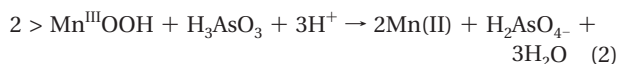
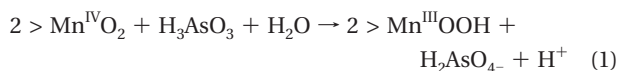
Density functional theory (DFT) calculations were used to investigate As(V) and As(III) surface complex structures and reaction energies on both Mn(III) and Mn(IV) sites in an attempt to better understand As(III) oxidation by birnessite, a layered Mn-dioxide mineral. Edge-sharing dioctahedral Mn(III) and Mn(IV) clusters with different combinations of surface functional groups ( $>MnOH$  and  $>MnOH_2$ ) were employed to mimic pH variability. Results show that As(V) adsorption was more thermodynamically favorable than As(III) adsorption on both Mn(III) and Mn(IV) surface sites under simulated acidic pH conditions. Therefore, we propose that As(V) adsorption inhibits As(III) oxidation by blocking adsorption sites. Under simulated acidic pH conditions, Mn(IV) sites exhibited stronger adsorption affinity than Mn(III) sites for both As(III) and As(V). Overall, we hypothesize that Mn(III) sites are less reactive in terms of As(III) oxidation due to their lower affinity for As(III) adsorption, higher potential to be blocked by As(V) complexes, and slower electron transfer rates with adsorbed As(III). Results from this study offer an explanation regarding the experimental observations of Mn(III) accumulation on birnessite and the long residence time of As(III) adsorption complexes on manganite ( $r$ -MnOOH) during As(III) oxidation.

## Introduction

Arsenic (As) is a toxic element with a maximum concentration level in drinking water set to 10 ppb by the U.S. Environmental Protection Agency. Arsenic contamination results from both anthropogenic and natural sources (1). The fate and transport of As in the environment, and its removal from drinking water, have been the subject of numerous investigations (2–13). Compared to arsenate (As(V)), arsenite (As(III)) is more toxic and mobile. Hence, the transformation of As(III) to As(V) not only decreases the toxicity of As, but also enhances As removal from drinking water and sequestration

to soils and sediments. As(III) can be oxidized to As(V) by manganese oxides (8), which are strong oxidants present in many soils and sediments. However, the oxidation mechanisms of As(III) by manganese oxides are not currently well understood.

Experimental studies have been conducted to investigate As (As(V) and As(III)) adsorption and oxidation by Mn(IV)-oxides and Mn(III)-(hydr)oxides (4, 5, 7–9, 11–15). Based on X-ray photoelectron spectroscopy (XPS) (7), Mn(IV) reduction to Mn(II) by As(III) is believed to proceed in two steps whereby two electrons are transferred from one As(III) molecule to two Mn(IV) cations that are subsequently reduced to Mn(III) [eq 1]. The two newly formed Mn(III) cations accept two additional electrons from another As(III) molecule and are reduced to Mn(II) cations [eq 2]. The following reactions correspond to the two steps at approximately pH 5 (7).



The intermediate Mn(III) cations are thought to be less reactive than Mn(IV) cations (7, 12) for As(III) oxidation.

The Mn(II) and As(V) products are released to the solution phase or re-adsorbed on the mineral surfaces. During As(III) oxidation, Mn(II), As(V), and As(III) can coexist in the solution phase and the surface cation sites can be a mixture of both Mn(IV) and Mn(III) (7). As(V) and Mn(II) may also compete with As(III) for surface sites and potentially block As(III) adsorption and inhibit its oxidation (4, 15). Mn(III) sites can compete with Mn(IV) sites for adsorption of aqueous species. Consequently, this chemical system becomes highly complex as the reaction progresses beyond the initial adsorption of As(III).

Key to elucidating the oxidation mechanisms of As(III) is ascertaining As(III) initial adsorption complexes (bidentate–binuclear (BB) or monodentate–mononuclear (MM)), which are the precursors to its oxidation. As(III) oxidation occurs very rapidly (9), unlike selenite (Se(IV)) (5), such that As(III) adsorption complexes on Mn(III,IV)-oxides are not easily measured or differentiated from As(V) adsorption complexes, using techniques such as extended X-ray absorption fine structure (EXAFS) spectroscopy (6).

Quantum chemical calculations complement experimental studies and can aid the interpretation of reaction mechanisms because stable intermediates such as As(III) complexes on Mn-oxides can be modeled. Density functional theory (DFT) has been applied to investigate various geochemical processes such as reactions occurring at the mineral–water interface (3, 16–23). By comparing calculated geometries, vibrational modes, and/or relative adsorption energies to experimental observations, quantum chemical calculations can help identify adsorption complexes. EXAFS spectroscopy in conjunction with DFT calculations have shown that As(III,V) mainly forms BB complexes on the surfaces of Fe- and Al-oxides (3, 14, 20, 24).

Birnessite (a layered MnO<sub>2</sub>) and manganite ( $r$ -MnOOH) (Figure 1), dominant Mn(III,IV)-oxides found in nature, have been used in experimental studies to mimic environmental redox processes. Hydroxyl groups on the basal plane of birnessite are doubly or triply coordinated to Mn atoms and inert in terms of exchange by oxyanions (25). Edge sites of birnessite, i.e., singly bound Mn surface functional groups

\* Corresponding author phone: (302) 831-1230; fax: (302) 831-0605; e-mail: mzhu@udel.edu.

<sup>†</sup> University of Delaware.

<sup>‡</sup> DuPont Crop Protection.

<sup>§</sup> The Pennsylvania State University.

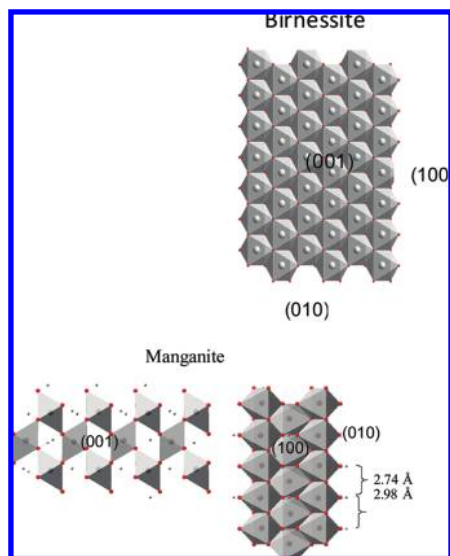


**FIGURE 1.** Crystal surfaces of manganite and a single layer of birnessite. Two Mn–Mn distances exist in manganite. Based on its slightly higher affinity for  $\text{HAsO}_4^{2-}$  adsorption (data not shown), the surface cluster with a 2.74 Å Mn–Mn distance was adopted for adsorption complexes involving Mn(III).

on the (100) and (010) faces (Figure 1), are therefore responsible for oxyanion adsorption, such as As(V) (3, 5, 11) and Se(IV) adsorption (5). According to the 1-p $K_a$  surface complexation model (SCM), edge sites of birnessite (25) or the predominant crystal faces of manganite (26) consist of >Mn–OH and >Mn–OH<sub>2</sub> (without >Mn–O) over a wide pH range.

In this study, the geometries and adsorption energies of As(III) and As(V) adsorption complexes on Mn(III) and Mn(IV) sites (or surface sites of manganite and birnessite) were calculated with DFT to better understand As(III) oxidation by Mn-oxides. The objectives of this study are to (1) compare Mn(III) and Mn(IV) sites in terms of As(III) adsorption and oxidation; (2) investigate the ability of As(V) to inhibit As(III) adsorption and its oxidation via competition for surface sites; and (3) provide molecular-level insight into oxyanion adsorption mechanisms on mineral surfaces.

## Materials and Methods

This study follows a methodology similar to that used by Kwon and Kubicki (17) and Paul et al. (19) for modeling oxyanions adsorbed on metal-oxides. All calculations were performed with Gaussian 03 (27), using the unrestricted, open-shell UB3LYP (28, 29) method. Calculations involved edge-sharing dioctahedral Mn-(hydr)oxide clusters surrounded by a small number of explicit H<sub>2</sub>O molecules to simulate short-range hydration. The high-spin states of Mn(III) ( $s = 4/2$ ) and Mn(IV) ( $s = 3/2$ ) were specified for the Mn-containing clusters.

Stoichiometrically balanced reactions were modeled to estimate the relative Gibbs free energy changes ( $\Delta G$ ) for As(III,V) adsorption on variably charged Mn(III,IV)-(hydr)oxide clusters. In addition to nondeprotonation adsorption reactions, in which adsorbed As(III,V) complexes do not release H<sup>+</sup>, deprotonation reactions of As(III,V) adsorption complexes were also considered to account for possible adsorption-induced H<sup>+</sup> release by As(III,V). Charges on each Mn(III,IV)-(hydr)oxide reactant were varied by adjusting the ratio of HO<sup>-</sup>/H<sub>2</sub>O functional groups terminating the cluster models. Charges on Mn(III,IV)-(hydr)oxide reactants ranged from +2 to 0, corresponding to a simulated pH range from acid to alkaline conditions (25, 26). H<sub>2</sub>AsO<sub>4</sub><sup>-</sup> and HAsO<sub>4</sub><sup>2-</sup> species of As(V) and H<sub>3</sub>AsO<sub>3</sub> and H<sub>2</sub>AsO<sub>3</sub><sup>-</sup> species of As(III)

were considered in the adsorption reactions because of their prevalence under environmentally relevant pH conditions.

As(V) BB configurations were chosen as the only adsorption complexes on the surface of the Mn(IV)-(hydr)oxide clusters based on EXAFS spectroscopic results (3, 5, 30). Because EXAFS studies of As(V) adsorption on Mn(III)-oxides and As(III) adsorption on either Mn(III)- or Mn(IV)-oxides have not been reported in the literature, MM adsorption was considered in addition to BB adsorption. Outer-sphere complexes were not included in this study and assumed not to lead to electron transfer between As(III) and Mn-oxides, although outer-sphere complexes are important for As(V) adsorption on mineral surfaces (31) and outer-sphere electron transfer can occur (32).

To estimate the relative Gibbs free energies for As(III,V) adsorption on Mn(IV) model surfaces, model reactants and products were first energy-minimized without symmetry or geometrical constraints in the gas phase (16, 19). Mn(III) model clusters were frozen (described below) during optimizations due to potential deficiencies of the DFT method in predicting correct Jahn–Teller distortions (33). For the purpose of comparing Mn(III) and Mn(IV) sites in terms of As adsorption, some Mn(IV) model clusters were also frozen. The frozen model surfaces for Mn(III) and Mn(IV) were constructed from the manganite (010) surface (ICSD-27457) and the birnessite (100) surface (ICSD-68916), respectively, from the Inorganic Crystal Structure Database (ICSD, Fachinformationszentrum Karlsruhe (FIZ) and National Institute of Standards and Technology (NIST)). Only the edge-sharing Mn<sub>2</sub>O<sub>8</sub> surface clusters were frozen during energy minimizations whereas all other atoms were relaxed including the H atoms used to neutralize the clusters. The electronic internal energies, instead of Gibbs free energies, were estimated for the complexes optimized with the frozen surface.

The all-electron 6-31G(d) basis set for all the elements (As, Mn, O, and H) or LanL2DZpd (34) for As and Mn, and 6-31G(d) for O and H (LanL2DZpd//6-31G(d)), were used to fully optimize the cluster geometries and provide thermal energy corrections (16, 17). For the clusters with frozen surfaces (Mn<sub>2</sub>O<sub>8</sub> clusters), the LanL2DZpd//6-31G(d) basis set combination was used to partially optimize the geometries. Single-point energy calculations were performed on each geometry-optimized (fully and partially) gas-phase species, using the 6-311++G(df, pd) basis set in combination with the Integral Equation Formalism Polarized Continuum Model (IEFPCM) (35) to account for long-range implicit hydration. For some As(III) complexes, natural population analysis (NPA) and natural bond orbital (NBO) (36) analyses were carried out with the same calculation method as the single-point energy calculations. The Gibbs free energies were estimated by the combination of the single-point electronic internal energies at the 6-311++G(df, pd) level and the zero-point and thermal energy corrections obtained from frequency calculations on the fully relaxed structures at the 6-31G(d) level. It is noteworthy that the predicted Gibbs free energies are conservatively accurate to  $\pm 20$  kJ/mol based on previous studies (19); however, relative energies for systems of the same composition should predict the relative enthalpies correctly.

## Results and Discussion

**Structures of As(III,V) Adsorption Complexes.** *Relaxed Surface Model versus Frozen Surface Model.* The relaxed surface model (i.e., fully energy-minimized) has been more frequently used in predicting surface adsorption complexes (16, 17, 19, 21–23). The frozen surface model (i.e., partially energy-optimized) neglects surface relaxation, whereas the relaxed surface model tends to exaggerate relaxation when the cluster is not large enough to minimize boundary effects. The configurations predicted by the two models should

**TABLE 1. Partially Energy-Optimized Geometries for As(III,V) Adsorption Complexes on Mn(III) and Mn(IV) Sites at the UB3LYP/LanL2DZpd//6-31G(d) Level of Theory**

Mn(IV) sites			
surface species	HAsO <sub>4</sub> (BB)	HAsO <sub>3</sub> (BB)	H <sub>2</sub> AsO <sub>3</sub> (MM) <sup>a</sup>
average $d_{As-O}$ (Å)	1.71	1.81	1.83
$d_{As-Mn}$ (Å)	3.18/3.21	3.22/3.23	3.35
Mn(III) sites			
surface species	HAsO <sub>4</sub> (BB)	H <sub>2</sub> AsO <sub>4</sub> (MM) <sup>b</sup>	HAsO <sub>3</sub> (BB)
average $d_{As-O}$ (Å)	1.71	1.70	1.82
$d_{As-Mn}$ (Å)	3.29/3.47	3.72	3.28/3.47

<sup>a</sup> With the neighboring functional group as >Mn(IV)-OH.

<sup>b</sup> With the neighboring functional group as >Mn(III)-OH<sub>2</sub>. The experimentally measured As(V)-O and As(V)-Mn(IV) distances are 1.68–1.69 and 3.16–3.22 Å, respectively (Manning et al. (3), Foster et al. (5), and Manceau et al. (30)).

be able to bracket experimental observations. A slight distortion was observed in the adsorption complexes involving the Mn(IV) cluster for the relaxed surface model, while a much higher distortion occurred for the Mn(III) complex (Figure S1, Table S1, and Table S2). In spite of ~0.1 Å longer Mn(IV)-Mn(IV) distances predicted by the relaxed model compared to the frozen model, the two models predicted similar average As(III,V)-Mn(IV) distances in BB adsorption configurations (Table S1), whereas the frozen surface model predicted slightly longer As(III)-Mn(IV) distances in the H<sub>2</sub>AsO<sub>3</sub> MM adsorption complex (Table S1).

**Average As-Mn and As-O Distances.** The As-Mn and As-O distances are the most important predicted geometric parameters because they can be directly measured by experimental techniques such as EXAFS spectroscopy (3, 5, 30). Both the predicted As(V)-O bond distances and the As(V)-Mn(IV) interatomic distances in the BB configuration (Table 1), regardless of its protonation state, agreed well with EXAFS spectroscopic measurements (3, 5, 30), which supports the formation of As(V) BB adsorption complexes. The predicted As(III)-Mn(III,IV) interatomic distances were similar to the corresponding As(V)-Mn(III,IV) interatomic distances in the BB configuration (Table 1). This is unlike As(III,V) adsorption on Al(III)- and Fe(III)-oxide surfaces whereby significant differences exist between As(III)-(Fe,Al) and As(V)-(Fe,Al) distances in BB configurations (3, 20, 24). As(III,V) complexes on the Mn(III) sites had much longer As-Mn interatomic distances than those formed on Mn(IV) sites due to the Jahn-Teller distortion of Mn(III) octahedra (Table 1, Figure 2a and b). The As(V)-Mn(III) distance in the MM configuration was 3.72 Å (Table 1), similar to the observation of 3.6 Å in As(V) MM complexes on Fe(III)-oxide surfaces (20). As(III)-Mn(III,IV) distances in the MM configuration were close to those in the BB configuration (Table 1) because the As atom faced the neighboring functional group (Figure 2c). Additional geometric parameters are listed in Tables S1 and S2.

**Effects of Protonation States on Adsorption Geometries.** Adsorption experiments are typically conducted under different pH conditions that can affect the protonation states of adsorbed species. The effects of protonation on the geometries of adsorbed As(III,V) complexes on the Mn(IV)-(hydr)oxide clusters were examined at the 6-31G(d) level of theory with the relaxed surface model (Table 1 and Table S1). Deprotonation of As(III) and As(V) resulted in only slight changes to the predicted As(III,V)-Mn(IV) and average As(III,V)-O distances in BB and MM adsorption

complexes (Table 1). However, upon deprotonation, the (Mn(IV))O-As-O(Mn(IV)) angles and the interatomic (Mn)O-O(Mn) distances in BB adsorption complexes changed significantly for As(V) complexes, but subtly for As(III) complexes (Table S1), implying a more rigid structure for As(III) complexes. The Mn-O(As(V)) distance in BB configurations decreased significantly from 2.00 to 1.87 Å with complete deprotonation (Table S1), indicating stronger interactions between the deprotonated adsorbates and the cluster model. On the other hand, the Mn-O(As(III)) distances remained nearly identical regardless of the protonation states (Table S1). The protonation states not only affected the geometries of As(III) in the MM configuration, but also rotated the As(III) complex, implying a more flexible MM configuration (Table S1).

**As(III,V) Adsorption Energies on Variably Charged Mn(IV) Clusters.** The calculated adsorption energies shown in Figure 3 (reaction equations are listed in Tables S3 and S4) enable a qualitative comparison to As pH adsorption envelopes. When comparing the nondeprotonation reactions, HAsO<sub>4</sub><sup>2-</sup> adsorption is much more thermodynamically favorable than H<sub>2</sub>AsO<sub>4</sub><sup>-</sup> adsorption (Figure 3). This is probably caused by the stronger electrostatic attraction between the doubly charged HAsO<sub>4</sub><sup>2-</sup> oxyanion and the Mn(IV) cluster compared to the singly charged H<sub>2</sub>AsO<sub>4</sub><sup>-</sup> oxyanion. For the deprotonation reactions, H<sub>2</sub>AsO<sub>4</sub><sup>-</sup> adsorption was more thermodynamically favorable than HAsO<sub>4</sub><sup>2-</sup> adsorption because less energy is required to break an O-H bond in H<sub>2</sub>AsO<sub>4</sub><sup>-</sup> than that in HAsO<sub>4</sub><sup>2-</sup> based on successive As(V) pK<sub>a</sub> values. A previous quantum chemical study also predicted that H<sub>2</sub>AsO<sub>4</sub><sup>-</sup> adsorption (deprotonation reaction) and HAsO<sub>4</sub><sup>2-</sup> adsorption (nondeprotonation reaction) on model Al- and Fe-oxides should be favorable (16). For As(III) adsorption, only nondeprotonation adsorption reactions were predicted to be thermodynamically favorable for both MM and BB configurations. This is attributable to the high pK<sub>a1</sub> of H<sub>3</sub>AsO<sub>3</sub> (9.3).

Figure 3a shows that the ΔG of deprotonation adsorption for H<sub>2</sub>AsO<sub>4</sub><sup>-</sup> and HAsO<sub>4</sub><sup>2-</sup> remained unchanged when decreasing the surface charge from +2 to +1, but increased (i.e., adsorption less favorable) when decreasing the surface charge from +1 to 0. On the other hand, the ΔG increased more abruptly for nondeprotonated H<sub>2</sub>AsO<sub>4</sub><sup>-</sup> and HAsO<sub>4</sub><sup>2-</sup> adsorption. Distinct adsorption trends were also observed for As(III) adsorption when decreasing the surface charge from +1 to 0: ΔG decreased for H<sub>3</sub>AsO<sub>3</sub> adsorption while ΔG increased for H<sub>2</sub>AsO<sub>3</sub> adsorption. From a macroscopic point of view, As(III) and As(V) pH adsorption envelopes tend to have maxima or inflection points at the pH near the pK<sub>a</sub> (H<sub>2</sub>AsO<sub>4</sub><sup>-</sup>/HAsO<sub>4</sub><sup>2-</sup> and H<sub>3</sub>AsO<sub>3</sub>/H<sub>2</sub>AsO<sub>3</sub><sup>-</sup>), which is a characteristic oxyanion adsorption pattern on mineral surfaces (2, 24, 37, 38).

The adsorption behavior of H<sub>2</sub>AsO<sub>4</sub><sup>-</sup>/HAsO<sub>4</sub><sup>2-</sup> and H<sub>3</sub>AsO<sub>3</sub>/H<sub>2</sub>AsO<sub>3</sub><sup>-</sup> in response to pH is dependent on whether the adsorption reactions release protons (38). Inner-sphere adsorption of oxyanions requires exchange with >Mn-OH and/or >Mn-OH<sub>2</sub> surface functional groups. A greater density of >Mn-OH functional groups is present on surfaces at high pH and does not favor ligand exchange since breaking a >Mn-OH bond requires more energy than breaking a >Mn-OH<sub>2</sub> bond. For adsorption reactions without H<sup>+</sup> release, such as HAsO<sub>4</sub><sup>2-</sup> and H<sub>2</sub>AsO<sub>4</sub><sup>-</sup> nondeprotonation adsorption, an increase in pH results in less favorable reactions (Figure 3a). Nevertheless, increasing pH can favor H<sup>+</sup> release by virtue of H<sub>2</sub>O formation of the released H<sup>+</sup> with hydroxyls on the surface or in solution. A large amount of H<sub>2</sub>O formation energy drives the reactions toward products. Additionally, the energy gained must be greater than the energy needed to exchange >Mn-OH vs >Mn-OH<sub>2</sub>. Paul (39) proposed H<sup>+</sup>-assisted ligand exchange to describe the role of H<sup>+</sup> in

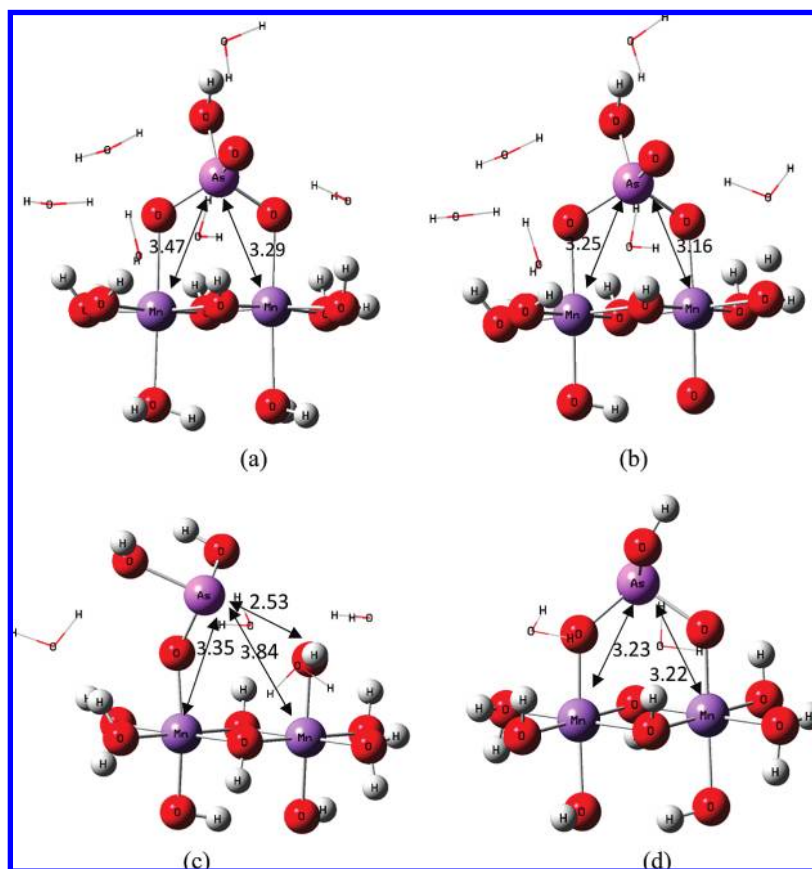


**FIGURE 2.** Some partially energy-minimized configurations (surface frozen model) of As(III) and As(V) surface adsorption complexes at the UB3LYP/LanL2DZpd//6-31G(d) level of theory: (a) bidentate–binuclear (BB)  $\text{HAsO}_4^{2-}$  adsorption on Mn(III); (b) bidentate–binuclear (BB)  $\text{HAsO}_4^{2-}$  adsorption on Mn(IV); (c) monodentate–mononuclear (MM)  $\text{H}_2\text{AsO}_3^-$  adsorption on Mn(IV); (d) bidentate–binuclear (BB)  $\text{HAsO}_3^-$  adsorption on Mn(IV). The explicit water molecules are shown as wires. The As–Mn interatomic distances are listed in angstroms (Å).

phosphate adsorption on Fe-oxide surfaces. Conceptually,  $\text{H}^+$  from  $\text{H}_2\text{PO}_4^-$  can react with an  $>\text{Fe}-\text{OH}$  surface functional group to form  $>\text{Fe}-\text{OH}_2$ , which is thermodynamically more favorable for ligand exchange with phosphate. This pathway may be applicable in  $\text{H}_3\text{AsO}_3$  adsorption (Figure 3b).

Increasing pH results in a larger number of  $>\text{Mn}-\text{OH}$  sites, a higher density of negative surface sites, and a higher extent of hydration (38). All of these factors disfavor oxyanion adsorption as pH increases. Although ligand exchange and hydration effects were mainly considered in the calculation strategy, the results qualitatively reflect the characteristics of oxyanion pH adsorption envelopes. This indicates that adsorption-induced  $\text{H}^+$  release is one reason for the maxima and inflection points observed in anion adsorption envelopes, although the oxyanion concentration is also an influencing factor (38).

**Electron Transfer versus Substitution Mechanisms.** In a classic electron transfer mechanism, As(III) must be first adsorbed as a surface complex and then oxidized (7). In a substitution mechanism, As(III) is directly oxidized through the transfer of a surface oxygen atom that bridges two Mn atoms to As(III) (7). Phosphate inhibits the adsorption and subsequent oxidation of As(III) on manganite (4). With a substitution mechanism (7), As(III) cannot be adsorbed as a stable surface complex on the bridging oxygen atoms (i.e., the substitution sites), and competitive oxyanions (e.g., phosphate) cannot block these sites by adsorption. As(III) oxidation through the substitution mechanism, therefore, may not be the most viable oxidation pathway. Additionally, As(III) adsorption and oxidation probably occurs on edge sites, which was supported by an atomic force microscopic

(AFM) study showing that birnessite dissolution by As(III) reduction occurred on edge sites (12).

**Comparison of As(III) and As(V) Adsorption.** A comparison of the adsorption affinities between As(III) and As(V) is demonstrated at pH 5 to assist in the interpretation of experimental observations (4, 7, 11, 12). Based on  $\text{p}K_a$  values ( $>\text{Mn}(\text{III})-\text{OH}_2$ ,  $\text{p}K_a = 8.20$ ; and  $>\text{Mn}(\text{IV})-\text{OH}_2$ ,  $\text{p}K_a = 4.31$ ) in the 1- $\text{p}K_a$  SCM (25, 26), the surface functional groups  $>\text{Mn}(\text{III})_2-(\text{OH})_2$  and  $>\text{Mn}(\text{IV})_2-\text{OH}_2(\text{OH})$  are assumed to be predominant at pH 5 on Mn(III) and Mn(IV) sites, respectively. According to the 1- $\text{p}K_a$  SCM, the point-of-zero-charge (PZC) of manganite is equivalent to the  $\text{p}K_a$ , i.e., 8.2; however, the  $\text{p}K_a$  of birnessite edge surface sites is not equivalent to birnessite PZC (PZC of  $\delta\text{-MnO}_2$  between 1.5–2.8 (40)) because birnessite charge is mainly caused by vacancy sites and Mn(III) substitution for Mn(IV) (25). At this pH, the aqueous As species are mainly  $\text{H}_2\text{AsO}_4^-$  and  $\text{H}_3\text{AsO}_3$ .

As(III) oxidation by Mn-oxides in batch experiments slows down with time and cannot be completed even if Mn-oxides are present in excess. At pH 5, As(V) BB adsorption is stronger than As(III) BB adsorption (Table 2 and Figure 3) on both Mn(III) and Mn(IV) sites, which is similar to As adsorption on Al- and Fe-oxides (14, 24). This indicates that the product, As(V), can block surface sites needed for As(III) oxidation and reduce its overall oxidation rate. A previous study has shown that the addition of phosphate significantly decreased As(III) oxidation on manganite (4). As(V) adsorption can have the same effect because the acid–base properties of As(V) and its affinity to mineral surfaces are similar to those of phosphate (11). Although As(V) inhibition decreases with pH, the inhibition from Mn(II), another reaction product, on

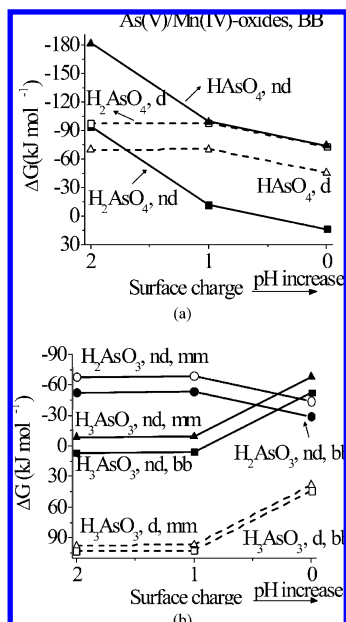


**FIGURE 3.** Reaction energies of As(V) (a) and As(III) (b) adsorption on variably charged surfaces of Mn(IV)-(hydr)oxide clusters. The deprotonation and nondeprotonation adsorption reactions are denoted as d and nd, respectively. BB and MM indicate bidentate–binuclear and monodentate–mononuclear adsorption, respectively.

As(III) oxidation becomes stronger as pH increases because Mn(II) sorption is enhanced (15) interfering with As(III) adsorption and subsequent oxidation (11).

**Comparison of Mn(III) and Mn(IV) Sites.** As(V) and As(III) adsorption on Mn(IV) sites is stronger than that on Mn(III) sites at pH 5 (Table 2). Additionally, the adsorption energy difference between As(V) and As(III) on Mn(IV) sites is much less than the difference between As(V) and As(III) adsorption on Mn(III) sites (Table 2). This suggests that As(V) adsorption could inhibit As(III) adsorption and oxidation more strongly on Mn(III) sites than on Mn(IV) sites. The stronger inhibition on Mn(III) sites may reduce As(III) oxidation by Mn(III) sites and contribute to Mn(III) accumulation on birnessite surfaces, as observed by XPS measurements (7) and in macroscopic batch experiments (12). On the other hand, at the same pH, Mn(IV) sites are less protonated than Mn(III) sites because of the lower  $pK_a$  of Mn(IV) sites; therefore, Mn(IV) sites may be preferred in Mn(II) sorption and can be blocked more severely than Mn(III) sites.

The surface functional groups on Mn(III) sites are more labile than the functional groups on Mn(IV) sites due to Jahn–Teller distortion (42), consistent with the predicted Mn(III,IV)-bond lengths (Table S5). The more labile surface functional groups lead to faster ligand exchange processes (41). Thus, As(V) and As(III) adsorption via ligand exchange occurs faster on Mn(III) sites than on Mn(IV) sites (42). Although the ligand exchange process on Mn(IV) sites is relatively slow, it is still fast based on the formation of inner-sphere adsorption complexes of As(V) and Se(IV) on the surfaces of Mn(IV)-oxides (3, 5). This can be attributed to the existence of the more labile  $>Mn(IV)-OH_2$  sites on edge surfaces of birnessite according to the  $1-pK_a$  SCM (25) and surface-enhanced ligand exchange rates on the solid surface (43).

The bond length of  $>Mn(IV)-O(As(III))$  (1.86 Å) is much shorter than the  $>Mn(III)-O(As(III))$  bond (2.05 Å) in the BB complex (Tables S1 and S2). The shorter distance may lead to a larger molecular orbital overlap and enhance the electron transfer rate from As(III) to Mn(IV) (42). NPA shows that the charge on the As atom is +1.64 and +1.55  $e^-$  in

**TABLE 2.** Estimated Reaction Energies of As(III,V) Adsorption at pH 5<sup>a</sup>

	reactions	$\Delta E$
BB	$H_2As^V O_4^-(H_2O)_{10} + [(OH)(H_2O)Mn^{IV}_2(OH)_6(H_2O)_3]^+ \rightarrow [HAs^V O_4 Mn^{IV}_2(OH)_6(H_2O)_8] + 7H_2O$	-75.08
BB	$H_2As^V O_4^-(H_2O)_{10} + [(H_2O)(H_2O)Mn^{III}_2(OH)_4(H_2O)_5]^+ \rightarrow [HAs^V O_4 Mn^{III}_2(OH)_4(H_2O)_{10}] + H^+(H_2O)_7$	-11.34
MM	$H_2As^V O_4^-(H_2O)_{10} + [(H_2O)(H_2O)Mn^{III}_2(OH)_4(H_2O)_5]^+ \rightarrow [H_2As^V O_4 Mn^{III}_2(OH)_4(H_2O)_{10}] + 7H_2O$	-43.26
BB	$H_3As^{III} O_3(H_2O)_6 + [(OH)(H_2O)Mn^{IV}_2(OH)_6(H_2O)_3]^+ \rightarrow [HAs^{III} O_3 Mn^{IV}_2(OH)_6(H_2O)_4] + H^+(H_2O)_7$	-47.19
BB	$H_3As^{III} O_3(H_2O)_6 + [(H_2O)(H_2O)Mn^{III}_2(OH)_4(H_2O)_5]^+ \rightarrow [HAs^{III} O_3 Mn^{III}_2(OH)_4(H_2O)_6] + 2[H^+(H_2O)_7] - 7H_2O$	128.95

<sup>a</sup> The functional groups  $>Mn(IV)(OH)(OH_2)$  and  $>Mn(III)(OH)_2$  were assumed. Energies are listed in kJ mol<sup>-1</sup>. Only HAsO<sub>3</sub> bidentate–binuclear (BB) adsorption configurations were considered for comparison of Mn(III) and Mn(IV) sites.

the HAsO<sub>3</sub> BB surface complexes on Mn(IV) and Mn(III) sites, respectively (Table S6). More electron density is apparently transferred from the HAsO<sub>3</sub> complex to the Mn(IV) surface (1.02) than to the Mn(III) surface (0.51) (Table S6). In addition, Mn(III) has a lower redox potential than Mn(IV) and electron transfer rates are strongly influenced by the difference in redox potential between the reductant and oxidant. Based on the above results and analysis, we are assuming that the rates of electron transfer between Mn(III) and As(III) are slower than those for Mn(IV) and As(III). We conclude that electron transfer could be the rate-limiting step for As(III) oxidation on Mn(III) sites. This suggests that As(III) surface complexes on Mn(III) sites could have a longer residence time such that the complexes can accumulate at a high concentration and be detected on manganite (4). Conversely, the rate-limiting step for As(III) oxidation on Mn(IV) sites, therefore, would be As(III) adsorption (11).

Mn(III) sites are less reactive at pH 5 than Mn(IV) sites in terms of As(III) oxidation. The reasons can be summarized by (1) Mn(III) sites have a lower affinity toward As(III) adsorption, (2) a higher tendency of Mn(III) sites to be blocked by As(V), and (3) likely slower electron transfer rates with adsorbed As(III). The reduced reactivity

of Mn(III) sites was also implied to some extent by experimental studies (7, 12). Thus, experimental conditions that favor intermediate Mn(III) production, such as increasing pH [eq 1 and eq 2], will reduce As(III) oxidation rates.

**Possible As(III) Oxidation Pathways.** Two As(III) adsorption complexes, MM and BB (Figure 2c and d), were considered as candidates for the precursor of As(III) oxidation. Both As(III) MM and BB complexes are possible precursors for oxidation on Mn(IV)-oxides although MM has more negative energy and is more likely (Figure 3). In the MM configuration, As(III) can first transfer one electron to the Mn(IV) cation on which it is adsorbed. The more positive As atom, due to the loss of one electron, can undergo nucleophilic substitution of the O atom in the next nearest functional group to become tetrahedral. Simultaneously, Mn(IV) bound to the next nearest functional group is reduced to Mn(III) via the substitution mechanism (7). If the electron transfer rate in a MM complex is slower, a BB complex could be formed from the MM complex and As(III) oxidation occurs via a classic electron transfer process. In terms of Mn(III)-oxide surfaces, only the BB mode was successfully predicted and may be the oxidation precursor.

### Acknowledgments

M.Z. is grateful for a graduate fellowship from the Institute of Soil and Environmental Quality at the University of Delaware and appreciates stimulating discussions with George W. Luther, III at the University of Delaware. All of the calculations were performed at the Delaware Biotechnology Institute (DBI) of the University of Delaware. The support for DBI is provided by Delaware EPSCoR through the Delaware Biotechnology Institute with funds from the National Science Foundation Grant EPS-0447610 and the State of Delaware.

### Note Added after ASAP Publication

Figure 1 was incorrect in the version of this paper published ASAP on July 17, 2009; the correct version published ASAP July 23, 2009.

### Supporting Information Available

Details regarding the calculated reaction energies, energy-minimized configurations, and NBO/NPA results are available free of charge via the Internet at <http://pubs.acs.org>.

### Literature Cited

- (1) Smedley, P. L.; Kinniburgh, D. G. A review of the source, behaviour and distribution of arsenic in natural waters. *Appl. Geochem.* **2002**, *17* (5), 517–568.
- (2) Raven, K. P.; Jain, A.; Loeppert, R. H. Arsenite and arsenate adsorption on ferrihydrite: Kinetics, equilibrium, and adsorption envelopes. *Environ. Sci. Technol.* **1998**, *32* (3), 344–349.
- (3) Manning, B. A.; Fendorf, S. E.; Bostick, B.; Suarez, D. L. Arsenic(III) oxidation and arsenic(V) adsorption reactions on synthetic birnessite. *Environ. Sci. Technol.* **2002**, *36*, 976–981.
- (4) Chiu, V. Q.; Hering, J. G. Arsenic adsorption and oxidation at manganite surfaces. I. Method for simultaneous determination of adsorbed and dissolved arsenic species. *Environ. Sci. Technol.* **2000**, *34*, 2029–2034.
- (5) Foster, A. L.; Gordon, E.; Brown, J.; Parks, G. A. X-ray absorption fine structure study of As(V) and Se(IV) sorption complexes on hydrous Mn oxides. *Geochim. Cosmochim. Acta* **2003**, *67* (11), 1937–1953.
- (6) Mitsunobu, S.; Takahashi, Y.; Uruga, T. Observation of chemical reactions at the solid-water interface by quick XAFS combined with a column reactor. *Anal. Chem.* **2006**, *78* (19), 7040–7043.
- (7) Nesbitt, H. W.; Canning, G. W.; Bancroft, G. M. XPS study of reductive dissolution of 7 Å-birnessite by  $H_3AsO_3$ , with constraints on reaction mechanism. *Geochim. Cosmochim. Acta* **1998**, *62* (12), 2097–2110.

- (8) Oscarson, D. W.; Huang, P. M.; Defosse, C.; Herbillon, A. Oxidative power of Mn(IV) and Fe(III) oxides with respect to As(III) in terrestrial and aquatic environments. *Nature* **1981**, *291* (5810), 50–51.
- (9) Parikh, S. J.; Lafferty, B. J.; Sparks, D. L. An ATR-FTIR spectroscopic approach for measuring rapid kinetics at the mineral/water interface. *J. Colloid Interface Sci.* **2008**, *320* (1), 177–185.
- (10) Pena, M.; Korfiatis, G.; Patel, M.; Lippincott, L.; Meng, X. Adsorption of As(V) and As(III) by nanocrystalline titanium dioxide. *Water Res.* **2005**, *39* (11), 2327–2337.
- (11) Scott, M. J.; Morgan, J. J. Reactions at oxide surfaces. 1. Oxidation of As(III) by synthetic birnessite. *Environ. Sci. Technol.* **1995**, *29*, 1898–1905.
- (12) Tournassat, C.; Charlet, L.; Boscach, D.; Manceau, A. Arsenic(III) oxidation by birnessite and precipitation of manganese(II) arsenate. *Environ. Sci. Technol.* **2002**, *36*, 493–500.
- (13) Feng, X.; Zu, Y.; Tan, W.; Liu, F. Arsenite oxidation by three types of manganese oxides. *J. Environ. Sci.* **2006**, *18* (2), 292–298.
- (14) Manning, B. A.; Fendorf, S. E.; Goldberg, S. Surface structures and stability of arsenic(III) on goethite: Spectroscopic evidence for inner-sphere complexes. *Environ. Sci. Technol.* **1998**, *32* (16), 2383–2388.
- (15) Power, L. E.; Arai, Y.; Sparks, D. L. Zinc adsorption effects on arsenite oxidation kinetics at the birnessite–water interface. *Environ. Sci. Technol.* **2005**, *39* (1), 181–187.
- (16) Kubicki, J. D.; Kwon, K. D.; Paul, K. W.; Sparks, D. L. Surface complex structures modeled with quantum chemical calculations: carbonate, phosphate, sulphate, arsenate and arsenite. *Eur. J. Soil Sci.* **2007**, *58*, 932–944.
- (17) Kwon, K. D.; Kubicki, J. D. Molecular orbital theory study on surface complex structures of phosphates to iron hydroxides: Calculation of vibrational frequencies and adsorption energies. *Langmuir* **2004**, *20*, 9249–54.
- (18) Ladeira, A. C. Q.; Ciminelli, V. S. T.; Duarte, H. A.; Alines, M. C. M.; Ramos, A. Y. Mechanism of anion retention from EXAFS and density functional calculations: Arsenic(V) adsorbed on gibbsite. *Geochim. Cosmochim. Acta* **2001**, *65* (8), 1211–1217.
- (19) Paul, K. W.; Kubicki, J. D.; Sparks, D. L. Quantum chemical calculations of sulfate adsorption at the Al- and Fe-(Hydr)oxide- $H_2O$  interfaces estimation of Gibbs free energies. *Environ. Sci. Technol.* **2006**, *40*, 7717–7724.
- (20) Sherman, D. M.; Randall, S. R. Surface complexation of arsenic(V) to iron(III) (hydr)oxides: Structural mechanism from ab initio molecular geometries and EXAFS spectroscopy. *Geochim. Cosmochim. Acta* **2003**, *67* (22), 4223–4230.
- (21) Zhang, N.; Blowers, P.; Farrell, J. Evaluation of density functional theory methods for studying chemisorption of arsenite on ferric hydroxides. *Environ. Sci. Technol.* **2005**, *39* (13), 4816–22.
- (22) Paul, K. W.; Borda, M. J.; Kubicki, J. D.; Sparks, D. L. Effect of dehydration on sulfate coordination and speciation at the Fe-(Hydr)oxide-water interface: A molecular orbital/density functional theory and Fourier transform infrared spectroscopic investigation. *Langmuir* **2005**, *21*, 11071–11078.
- (23) Paul, K. W.; Kubicki, J. D.; Sparks, D. L. Sulphate adsorption at the Fe (hydr)oxide- $H_2O$  interface: comparison of cluster and periodic slab DFT predictions. *Eur. J. Soil Sci.* **2007**, *58*, 978–988.
- (24) Arai, Y.; Elzinga, E. J.; Sparks, D. L. X-ray absorption spectroscopic investigation of arsenite and arsenate adsorption at the aluminum oxide-water interface. *J. Colloid Interface Sci.* **2001**, *235* (1), 80–88.
- (25) Peacock, C. L.; Sherman, D. M. Sorption of Ni by birnessite: Equilibrium controls on Ni in seawater. *Chem. Geol.* **2007**, *238*, 94–106.
- (26) Ramstedt, M.; Andersson, B. M.; Shchukarev, A.; Sjöberg, S. Surface properties of hydrous manganite ( $\gamma$ -MnOOH). A potentiometric, electroacoustic, and X-ray photoelectron spectroscopy study. *Langmuir* **2004**, *20*, 8224–8229.
- (27) Frisch, M. J. *Gaussian 03, Revision C.02*; Gaussian, Inc.: Wallingford, CT, 2004.
- (28) Lee, C.; Yang, W.; Parr, R. G. Development of the Colle-Salvetti correlation-energy formula into a functional of the electron density. *Phys. Rev. B* **1988**, *37* (2), 785–789.
- (29) Becke, A. D. Density-functional thermochemistry. 3. The role of exact exchange. *J. Chem. Phys.* **1993**, *98* (7), 5648–5652.
- (30) Manceau, A.; Lanson, M.; Geoffroy, N. Natural speciation of Ni, Zn, Ba, and As in ferromanganese coatings on quartz using X-ray fluorescence, absorption, and diffraction. *Geochim. Cosmochim. Acta* **2007**, *71* (1), 95–128.

- (31) Catalano, J. G.; Park, C.; Fenter, P.; Zhang, Z. Simultaneous inner- and outer-sphere arsenate adsorption on corundum and hematite. *Geochim. Cosmochim. Acta* **2008**, *72* (8), 1986–2004.
- (32) Rosso, K. M.; Morgan, J. J. Outer-sphere electron transfer kinetics of metal ion oxidation by molecular oxygen. *Geochim. Cosmochim. Acta* **2002**, *66* (24), 4223–4233.
- (33) Kaplan, I. G. Spin and orbital degeneracy problems in the DFT method. Relation to the Jahn-Teller effect. *J. Mol. Struct.* **2007**, *838* (1–3), 39–43.
- (34) Check, C. E.; Faust, T. O.; Bailey, J. E.; Wright, B. J.; Gilbert, T. M.; Sunderlin, L. S. Addition of polarization and diffuse functions to the LANL2DZ basis set for P-Block elements. *J. Phys. Chem. A* **2001**, *105*, 8111–8116.
- (35) Cancès, E.; Mennucci, B.; Tomasi, J. A new integral equation formalism for the polarizable continuum model: Theoretical background and applications to isotropic and anisotropic dielectrics. *J. Chem. Phys.* **1997**, *107* (8), 3032–3041.
- (36) Glendenning, E. D.; Reed, A. E.; Carpenter, J. E.; Weinhold, F. (<http://www.osc.edu/supercomputing/software/apps/gaussian03.shtml>).
- (37) Yao, W.; Millero, F. J. Adsorption of phosphate on manganese dioxide in seawater. *Environ. Sci. Technol.* **1996**, *30*, 536–541.
- (38) Hingston, F. J. A review of anion adsorption. In *Adsorption of Inorganics at Solid-Liquid Interfaces*; Anderson, M. A., Rubin, A. J., Eds.; Ann Arbor Science: Ann Arbor, MI, 1981; pp 51–90.
- (39) Paul, K. W. Molecular modeling study of sulfate and phosphate adsorption at the mineral-water interface. Ph.D Thesis, University of Delaware, Newark, DE, 2007.
- (40) Kinniburgh, D. G.; Jackson, M. L. Cation adsorption by hydrous metal oxides and clay. In *Adsorption of Inorganics at Solid-Liquid Interfaces*; Anderson, M. A., Rubin, A. J., Eds.; Ann Arbor Science: Ann Arbor, MI, 1981; pp 91–160.
- (41) Cotton, F. A.; Wilkinson, G. *Advanced Inorganic Chemistry*, 5th ed.; John Wiley & Sons: New York, 1988.
- (42) Nico, P.; Zasoski, A. J. Importance of Mn(III) Availability on the Rate of Cr(III) Oxidation on  $\delta$ -MnO<sub>2</sub>. *Environ. Sci. Technol.* **2000**, *34*, 3363–3367.
- (43) Wang, J.; Rustad, J. R.; Casey, W. H. Calculation of water-exchange rates on aqueous polynuclear clusters and at oxide-water interfaces. *Inorg. Chem.* **2007**, *46* (8), 2962–2964.

ES900537E